CHAPTER IV
RESULTS AND DISCUSSION

4.1 Characterization of Raw Materials

4.1.1 Structural Characterization of Natural Rubber Latex

Centrifuged Natural rubber latex (NR latex) with 60% dry rubber content was supplied from the Rubber Research Institute of Thailand, Bangkok, Thailand.

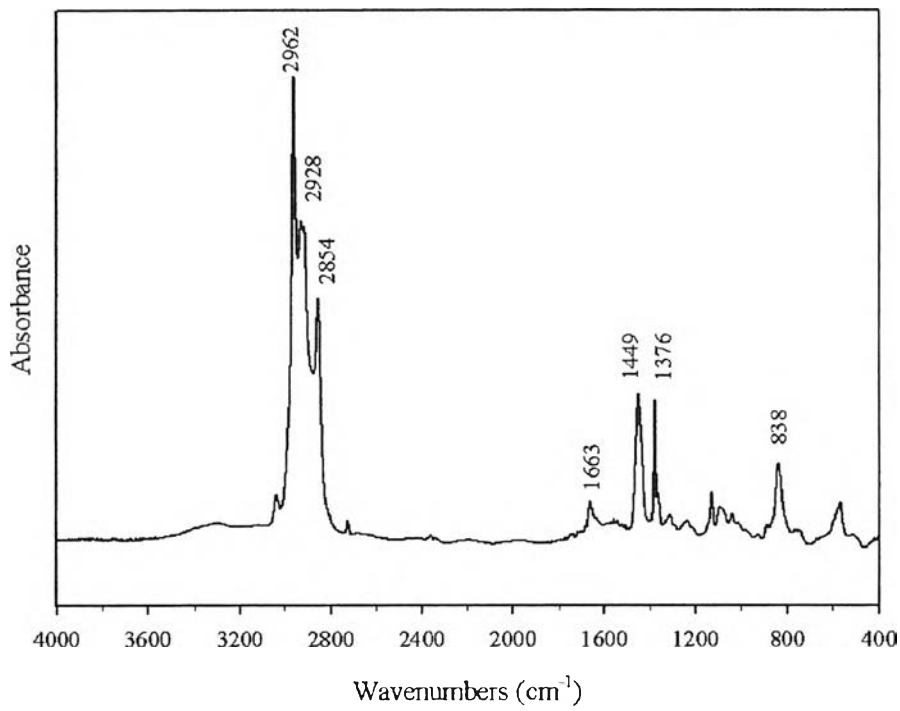

Figure 4.1 FTIR spectrum of natural rubber latex.

NR latex was characterized by using FTIR. The FTIR spectrum of NR was shown in Figure 4.1. The spectrum contains seven principal absorption peaks, characteristic of the well-known cis-1,4-polyisoprene structural of NR (Nor, 2000; Kang, 2000). The main characteristic peaks are summarized in Table 4.1.

Table 4.1 Characteristic adsorption peaks of NR latex

Wavenumbers (cm^{-1})	Vibration Assignment
2962	CH_3 asymmetric stretching
2928	CH_2 asymmetric stretching
2854	CH_2 symmetric stretching
1663	C=C stretching
1449	CH_2 deformation
1376	CH_3 asymmetric deformation
838	=C-H wagging

4.1.2 Structruction Characterization of Sodium Alginate

Sodium alginate (Carlo Erba Co., Ltd.) was used as a surface-active agent for the NR latex.

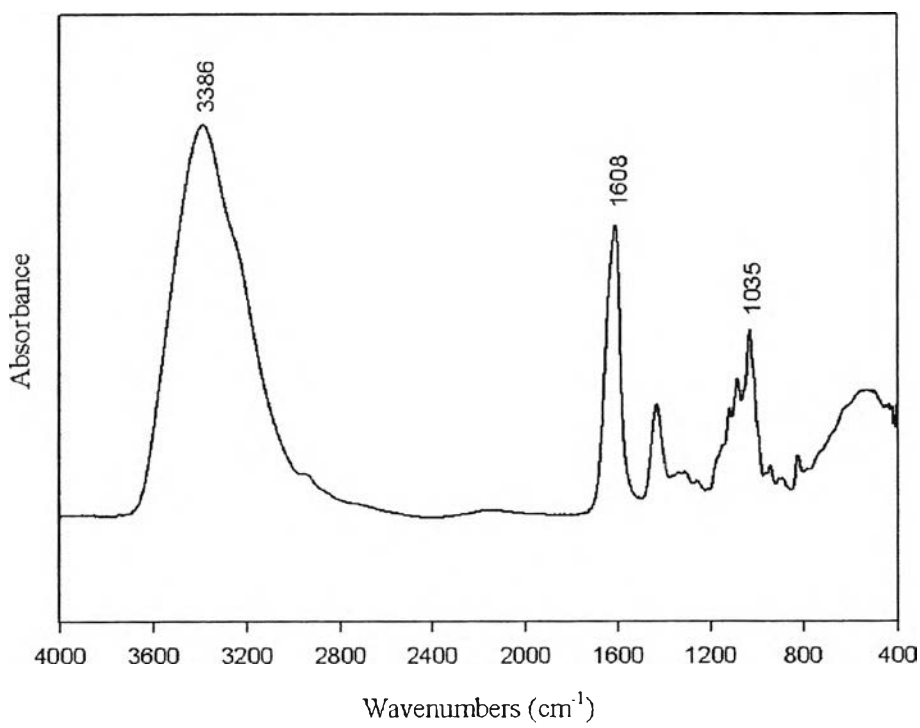

Figure 4.2 FTIR spectrum of Sodium alginate.

FTIR spectrum of alginate, the absorption characteristic peaks of alginate were observed at 3386, 1608 and 1035 cm^{-1} (Figure. 4.2) corresponded to hydroxyl, carbonyl and C-O-C bond in theirs structural unit, respectively (Parhi, 2006). The main characteristic peaks are summarized in Table 4.2.

Table 4.2 Characteristic adsorption peaks of sodium alginate

Wavenumbers (cm^{-1})	Vibration Assignment
3386	O-H stretching
1608	C=O stretching
1035	C-O-C stretching

4.1.3 Characterization of Synthesized Polyaniline

PANI was synthesized in its emeraldine base form according to the method described by Cao *et al.* (1989) (see experimental section for details).

4.1.3.1 Structural Characterization

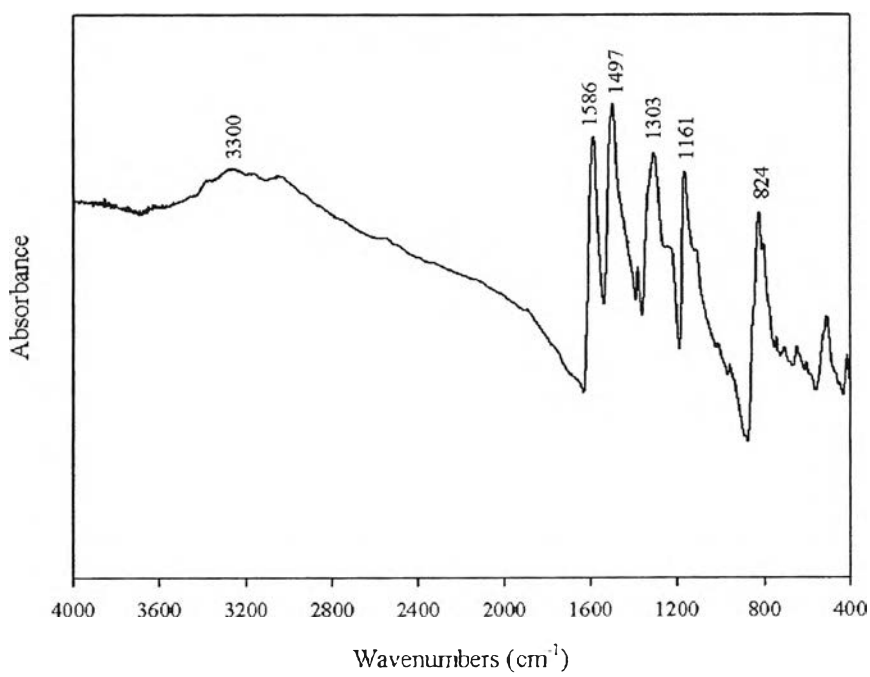

Figure 4.3 FTIR spectrum of polyaniline emeraldine base (PANI-EB) form.

Figure 4.3 shows the FTIR spectrum of synthesized PANI having identical absorption peaks as found in the earlier studies (Salaneck, 1993; Zeng, 1998). The main characteristic peaks are summarized in Table 4.3.

Table 4.3 Characteristic adsorption peaks of synthesized polyaniline emeraldine base

Wavenumbers (cm^{-1})	Vibration Assignment
3300	NH Stretching
1586	Stretching vibration of C=N quinoid ring
1497	Stretching vibration of C=C benzenoid ring
1303	Stretching vibration of C-N benzenoid ring
1161	vibration mode of quinoid ring
824	C-H bending vibration of para-couple benzene ring

4.1.3.2 Thermal Stability

The thermograms of undoped and doped PANI powder are shown in Figure 4.4. For the PANI-EB (undoped), the thermogram shows two discrete weight loss steps in the temperature ranges of 60-100°C and 480-600°C, corresponding to the loss of water and the degradation of PANI, respectively. The thermogram of PANI-ES (doped) exhibited three weight loss steps, which is similar to the observation done by Jeevananda *et al.* (2001). The first step in the range of 65-120°C is again explained with the loss of water. The second weight loss step between 120 and 280°C has been explained with the loss of low molecular weight polymer and unbounded HCl from PANI chains (Chan, 1989). The third weight loss step between 420-580°C is related to the degradation of PANI chains.

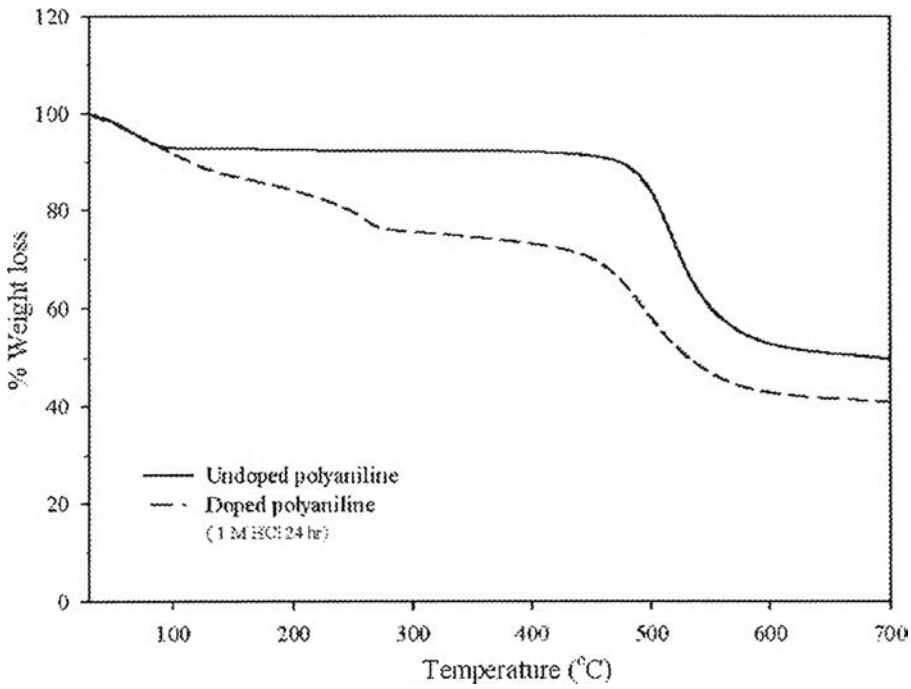

Figure 4.4 Thermal gravimetric analysis (TGA) thermogram of emeraldine base form (EB) (undoped) and emeraldine salt form (ES) (doped) of PANI.

4.1.3.3 Particle Size Analysis

The average particle diameter of PANI was determined to be approximately 20.76 μm with standard deviation of 0.1179 as shown in Table 4.4.

Table 4.4 The mean particle diameter of undoped PANI

Experiment	Mean particle diameter (μm)[a]
1	20.75
2	20.65
3	20.71
4	20.96
5	20.73
AVG	20.76
STD	0.1179

a: determined from D [4,3] mode

4.1.3.4 Scanning Electron Microscope (SEM)

SEM images in Figure 4.5 show the morphology of PANI powder prepared from chemical oxidative polymerization having small globular particles that usually can agglomerate to formed larger particle size.

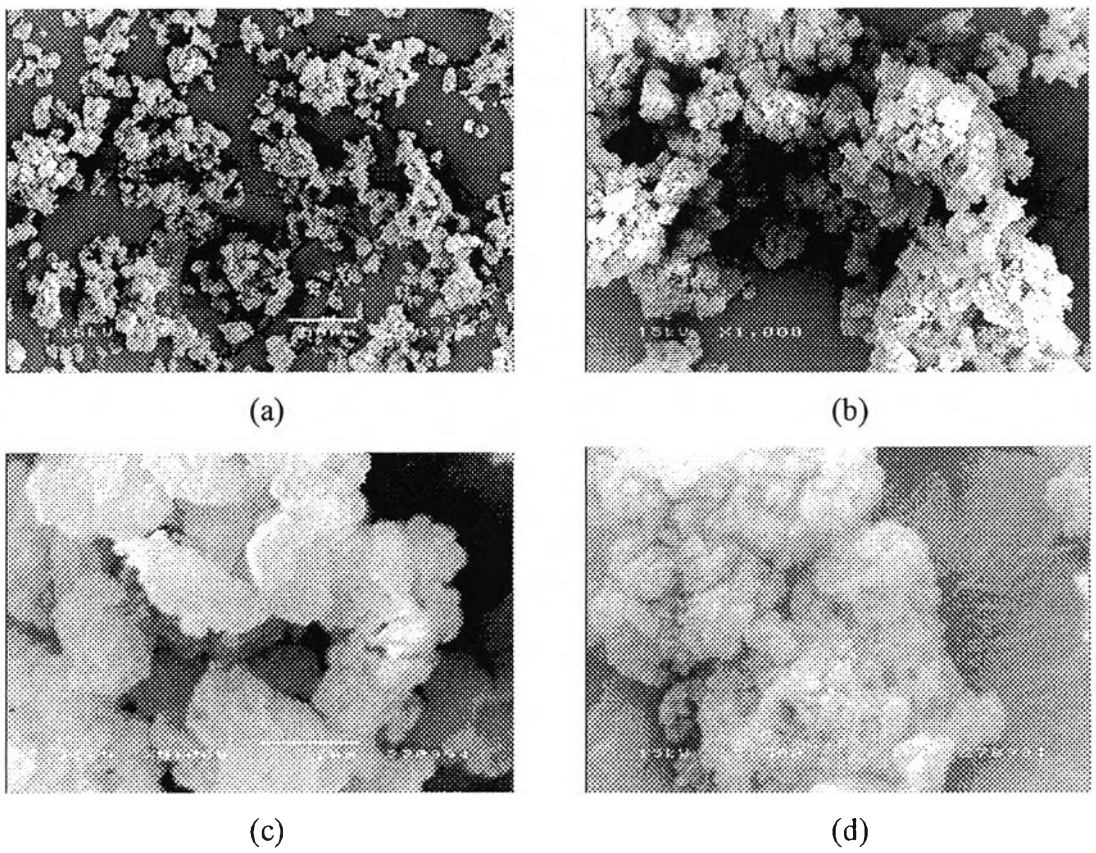

Figure 4.5 SEM micrographs of undoped PANI-EB powder at different magnification (a) x 350 (b) x 1000 (c) x 5000 and (d) x 7500.

4.2 Preparation and Characterization of Polyaniline/Natural Rubber Composite Fiber

4.2.1 Polyaniline/Natural Rubber Composite Fiber Spinning

The PANI/NR composite fibers were obtained in form of bundle fiber which each bundle fiber consist of many single fiber stick together. The cross-sectional shape of the resulting fiber bundles is roughly circular as shown in Figure

4.6. The average fiber bundle diameter are shown in Table 4.5, as determined from the SEM images of 90 selected fiber bundles with the help of image-analysis software (SemAfore 4.0). It should be noticed that for the determination of cross-sectional areas, voids or spaces in fiber bundles were neglected.

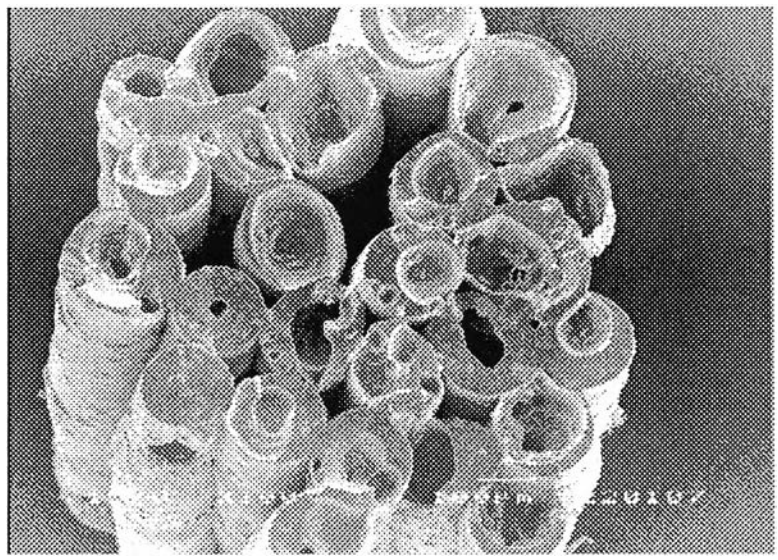

Figure 4.6 Scanning electron microscopy (SEM) image of the cross-section of a bundle of a PANI/NR composite fiber comprising 5% w/w PANI.

Table 4.5 The average diameter of polyaniline/natural rubber composite fiber

PANI content (% w/w)	Average diameter (mm)	
	Undoped PANI/NR composite fiber	HCl-doped PANI/NR composite fiber
0	0.840	0.831
0.5	0.861	0.831
1	0.894	0.808
2	0.872	0.847
5	0.819	0.888
10	0.856	0.842

4.2.2 Structural Characterization of Polyaniline/Natural Rubber Composite Fiber

The first level of characterization relied on Fourier transformation infrared (FTIR) spectra of neat PANI-EB, neat NR fibers (without PANI but comprising sodium alginate), and undoped PANI/NR composite fiber bundles are shown in Figure 4.7. The spectrum of the NR fibers shows the main absorption peaks at 2928, 2962, 2851, 1663, 1447, 1375 and 835 cm^{-1} (Table 4.6). Gratifyingly, these signals are characteristic of NR (Nor, 2000; Kang, 2000). Additional bands can be observed at 3373, 1629 and 1035 cm^{-1}, corresponding to hydroxyl, carbonyl and C-O-C stretching vibrations, associated with the sodium alginate in the fibers (Table 4.6) (Parhi, 2006). The spectrum of the neat PANI exhibits absorption peaks that mirror those reported for the emeraldine base form (undoped) of PANI in earlier studies (Salaneck, 1993; Zeng, 1998). The main characteristic peaks are summarized in Table 4.6.

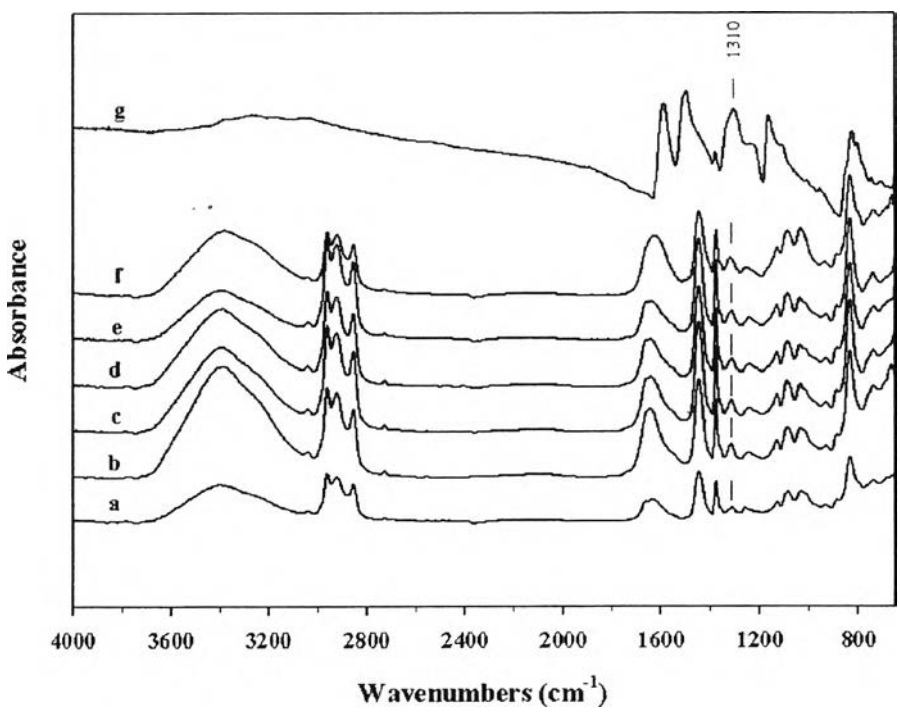

Figure 4.7 ATR-FTIR spectra of natural rubber (a); undoped PANI/NR composite fibers containing (b) 0.5, (c) 1, (d) 2, (e) 5, and (f) 10 % w/w of PANI; and undoped PANI (g).

Table 4.6 Wavenumbers (cm^{-1}) as observed in the FTIR spectra of NR, Alginate, undoped PANI and PANI/NR composite fibers

Wavenumber (cm^{-1})	Vibration Assignment	NR Latex	Sodium Alginate	PANI	NR/PANI composite
3373	O-H stretching		√		√
3300	NH stretching			√	
2962	CH_3 asymmetric stretching	√			√
2928	CH_2 asymmetric stretching	√			√
2854	CH_2 symmetric stretching	√			√
1663	C=C stretching	√			√
1629	C=O stretching		√		√
1586	Stretching vibration of C=N quinoid ring			√	
1497	Stretching vibration of C=C quinoid ring			√	
1447	CH_2 deformation	√			√
1375	CH_3 asymmetric deformaiton	√			√
1310	Stretching vibration of C-N quinoid ring			√	√
1161	Vibration mode of quinoid ring			√	
1035	C-O-C stretching		√		√
838	C-H bending vibration of para-couple benzene ring			√	
835	=C-H wagging	√			√

The characteristic absorption peaks of all three components (NR, sodium alginate, PANI) can also be found in the spectra of composite fibers with a PANI content of 0.5-10% w/w. The signals of PANI can not be unequivocally distinguished in the composites due to low PANI content in the composites and overlap with NR and sodium alginate signals. Nevertheless, the spectra of the PANI/NR composite fibers show an increase of the relative intensity of a peak around 1310 cm^{-1} with increasing PANI content. This signal is assigned to the stretching of the C-N of the benzenoid structure of PANI and is indicative for an increasing PANI concentration throughout the series.

4.2.3 Thermal Stability of Polyaniline/Natural Rubber Composite Fiber

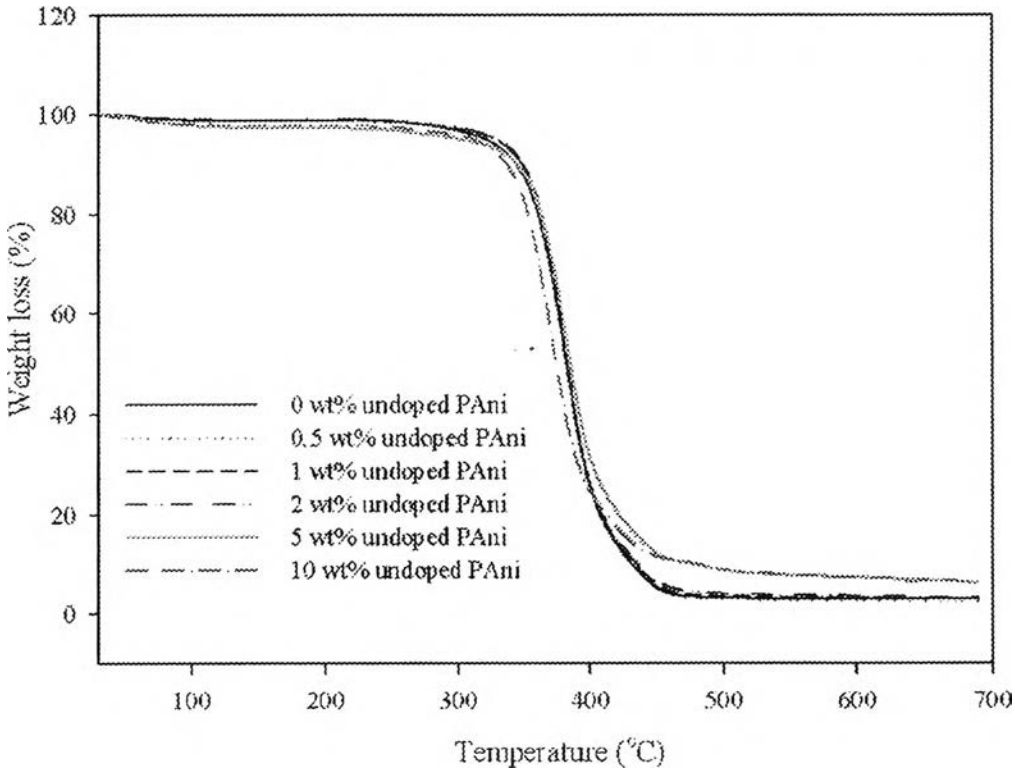

Figure 4.8 Thermogavimetric analysic (TGA) traces of bundles of neat NR fiber (comprising sodium alginate but no PANI) and the series of undoped PANI-EB/NR composite fibers.

The thermal stability of the fibers under investigation was probed by thermogravimetric dynamic temperature analyses, which were carried out under nitrogen at a heating rate of 10°C/min. The thermograms for the series of composite fibers are shown in Figure 4.8, together with the reference experiments for the neat PANI and the neat NR fiber. The thermogram of the neat NR fiber (without PANI but with sodium alginate) shows only one discrete weight loss step that is typical for the degradation of NR (Moreno, 2006) and sets in at around 320°C, is steepest around 370°C and is complete at a temperature of around 475°C with a char yield of 3.1490%. All composite fibers show virtually identical behavior. Concomitantly, the char yield continuously increases with increasing PANI content in the composites were observed. Gratifyingly, there was no remarkable change in the thermal stability of the composite fibers upon doping, as can be seen from the thermograms shown in Figure 4.9.

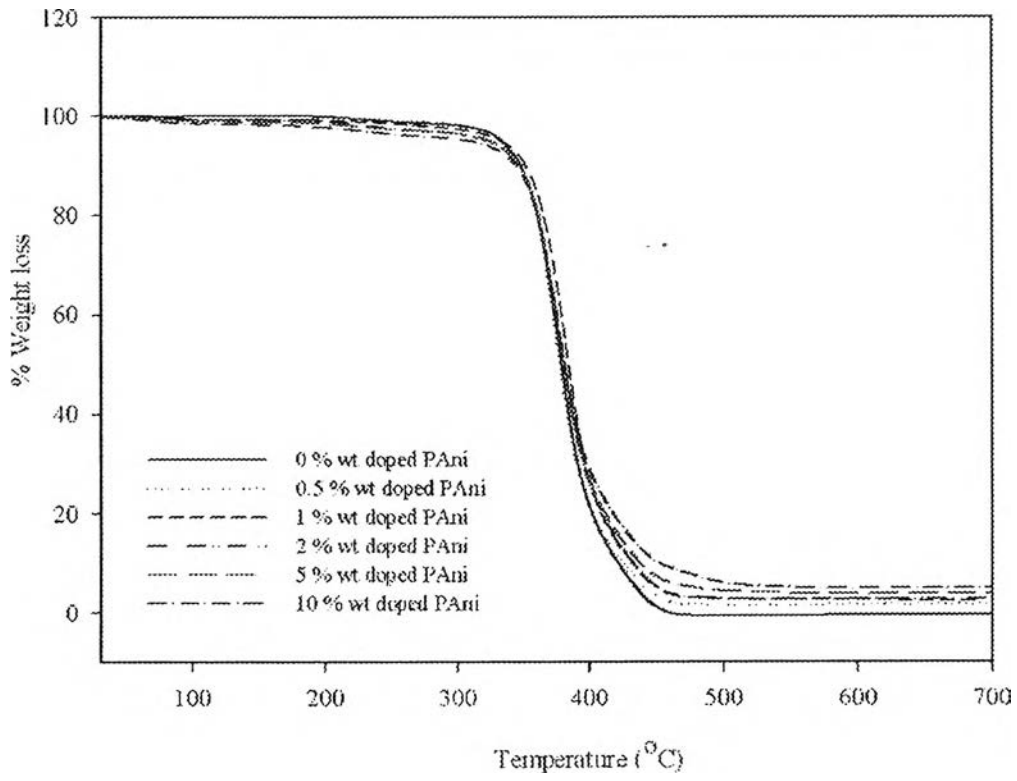

Figure 4.9 Thermogravimetric analysis (TGA) traces of bundles of neat NR fiber (comprising sodium alginate but no PANI) and the series of HCl-doped PANI-ES/NR composite fibers.

4.2.4 Morphology of Polyaniline/Natural Rubber Composite Fiber

Surface scanning electron microscopy (SEM) images of undoped and HCl-doped PANI/NR composite fiber bundles containing 5 and 10% w/w PANI and of a NR reference without PANI are shown in Figure 4.10. It was found that the roughness of the fiber surface increases somewhat with increasing PANI content. The surface roughness of the nanocomposite fiber appears to increase upon doping with HCl and the size of the features matches with the dimensions of the PANI particles. In order to further explore the distribution of the PANI particles throughout the fibers, cross-sections of freeze-fractured PANI/NR composite fibers containing 5 and 10% w/w PANI and of a neat NR reference fiber were imaged by SEM (Figure 4.11). In the case of the neat NR reference fiber (Figure 4.11a), a homogeneous morphology was observed. By contrast, the SEM images of the 5 and 10% w/w PANI-containing fibers show clear evidence of the presence of PANI particles. The images show a combination of well-dispersed, isolated PANI particles and agglomerates, which are typical for composites of ultimately rather incompatible components (Souza, 2006). Rather interestingly, the images (particularly of the 5% w/w HCl-doped PANI/NR fiber) suggest an inhomogeneous distribution with high local PANI particle/agglomerate densities (Figure 4.11b-right). It appears that the PANI preferentially resides at the surface of the fibers; this morphology may be the result of the very different polarities of the PANI and the NR and the coagulation process, which utilizes a polar solvent bath (methanol/$CaCl_2$, vide supra), providing a driving force for migration of PANI to the fiber surface during this step. Furthermore, it can be seen that the PANI particles in the SEM image of the 10% w/w HCl-doped PANI (Figure 4.11c-right) are more clearly observed than in the image of the undoped PANI (Figure 4.11c-left). This evidence may be presumably reflect whether the doping enhances the conductivity of PANI to allow for clearer in SEM observation.

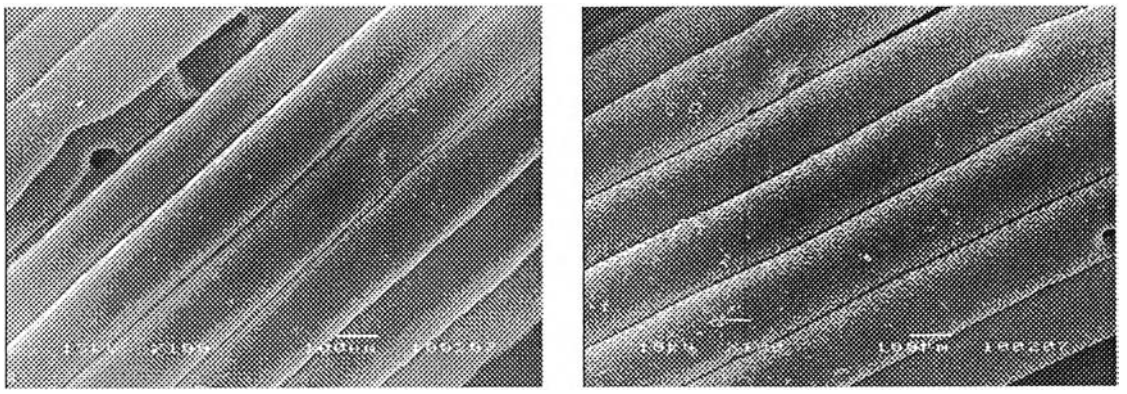

(a)

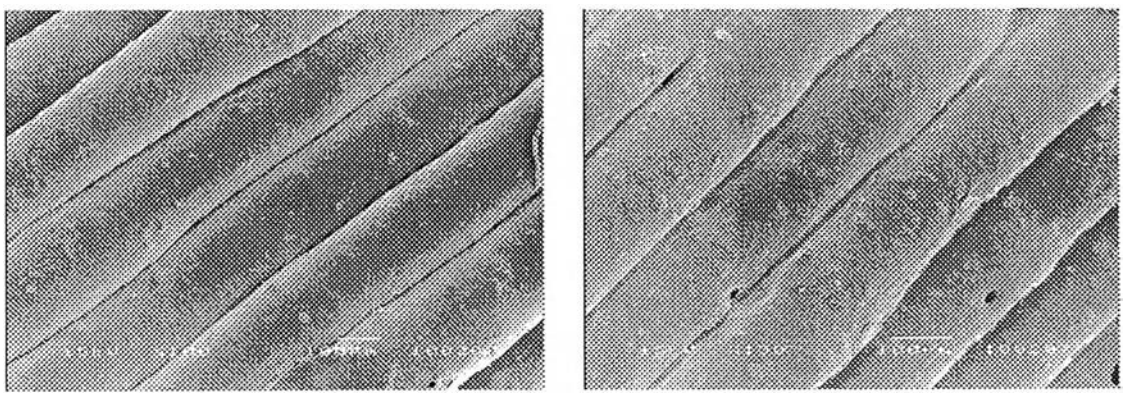

(b)

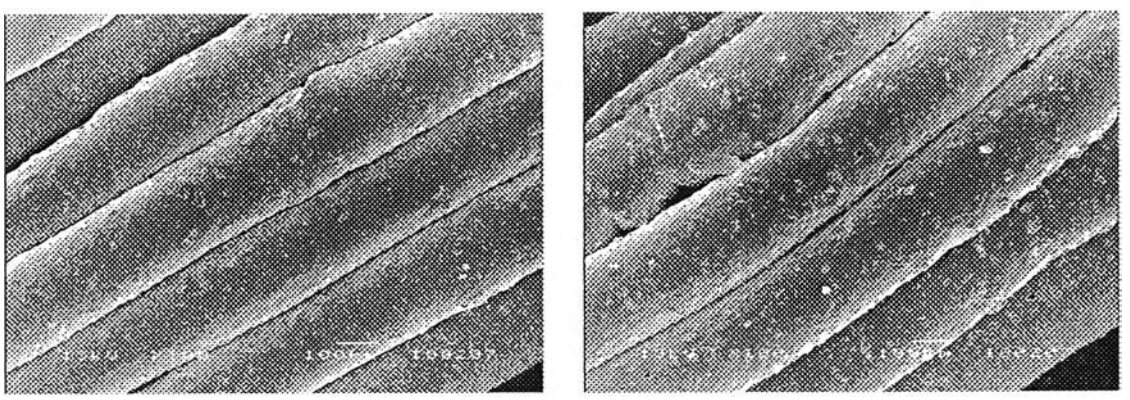

(c)

Figure 4.10 Scanning electron microscopy (SEM) images of the surface of bundles of undoped and HCl-doped PANI/NR composite fibers with PANI contents of (a) 0, (b) 5, and (c) 10% w/w; left column: undoped, right column: doped.

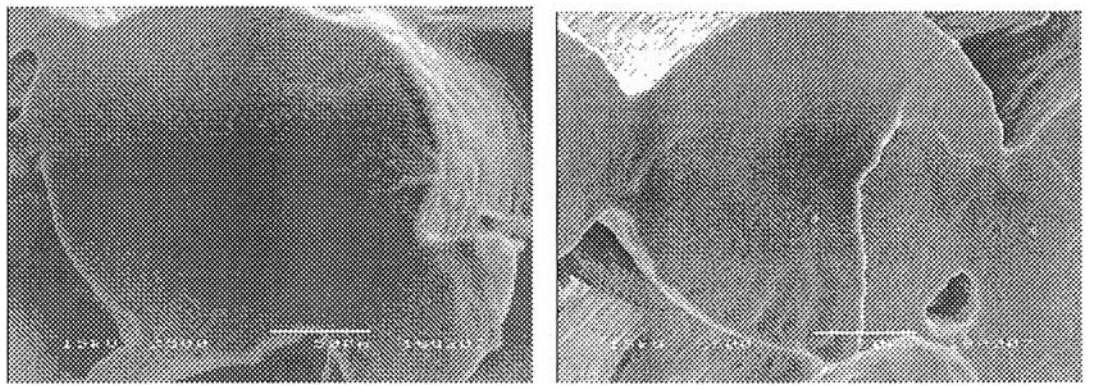

(a)

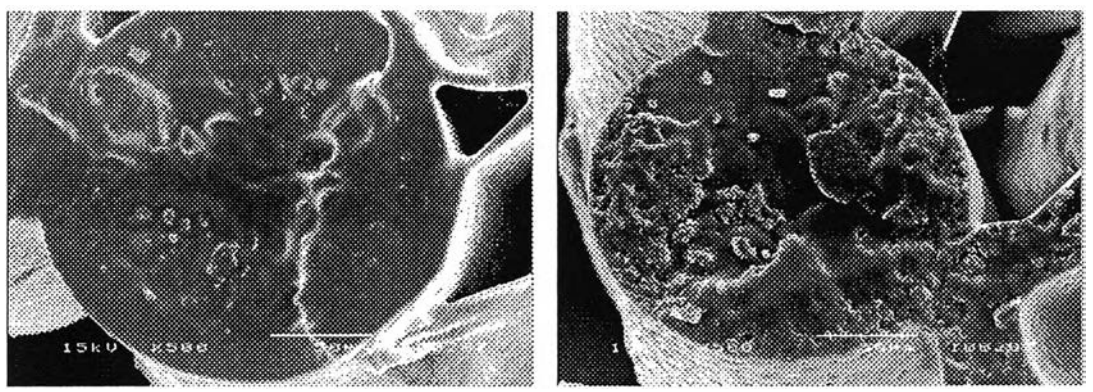

(b)

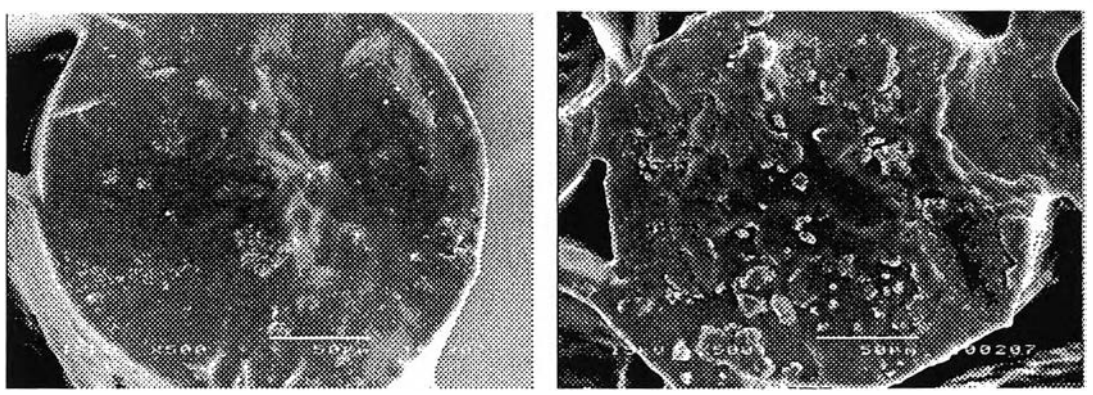

(c)

Figure 4.11 Scanning electron microscopy (SEM) images of cross-section of bundles of fractured, undoped and HCl-doped PANI/NR composite fibers with PANI contents of (a) 0, (b) 5, and (c) 10% w/w, left column: undoped, right column: doped.

4.2.5 Mechanical Properties of Polyaniline/Natural Rubber Composite Fiber

The mechanical properties of the undoped and doped PANI/NR composite fibers were determined by standard tensile testing experiments. The results are compiled in Figures 4.12 and 4.13. The neat NR fiber (without PANI) displays a tenacity of about 1 cN/tex and an elongation at break of 820%. These values are typical and reveal the mechanical characteristic of natural rubber (Hofmann, 1989). The tenacity (Figure 4.12) and elongation at break (Figure 4.13) are somewhat reduced upon the introduction of the PANI particles. In fact, tenacity and elongation at break seem to roughly linearly decrease with increasing PANI content to 0.306 cN/tex (tenacity) and 160% (elongation at break) at a PANI content of 10% w/w. Similar tendencies were found in previous work (Jeevananda, 2001) on ethylene-vinyl acetate copolymer/PANI composites and on styrene butadiene styrene TRI block copolymer/PANI composites (Souza, 2006). This situation may reflect the poor mechanical properties of PANI, the limited mechanical interaction between the NR matrix and the PANI filler, or the presence of microvoids in the matrix, which are observed in the SEM micrographs (Figure 4.10). Most interestingly, the tenacity and elongation at break of most of the PANI-containing samples increase again upon doping, in the case of the 10% w/w blend in a rather significant way to 0.500 cN/tex (tenacity) and 583% (elongation at break). The exact origin of this fortunate effect is as of yet unclear, but it may be related to electrostatic interaction (introduced by HCl doping) between the protonated PANI and the alginate network (Yu, 2006).

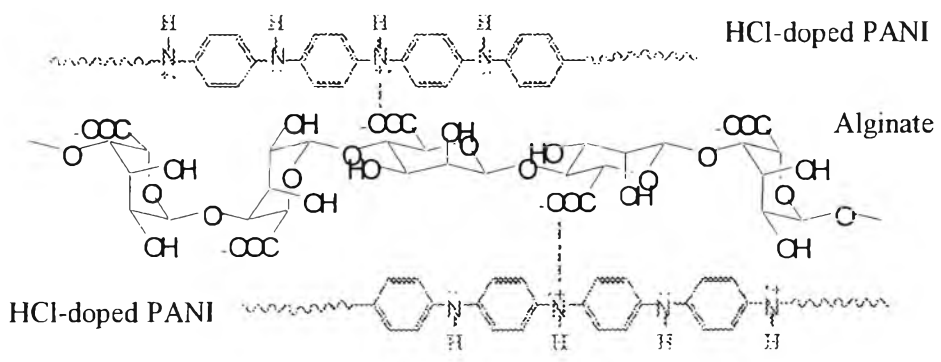

Schemce 4.1 Schematic drawn the electrostatic interaction between PANI chains and alginate network.

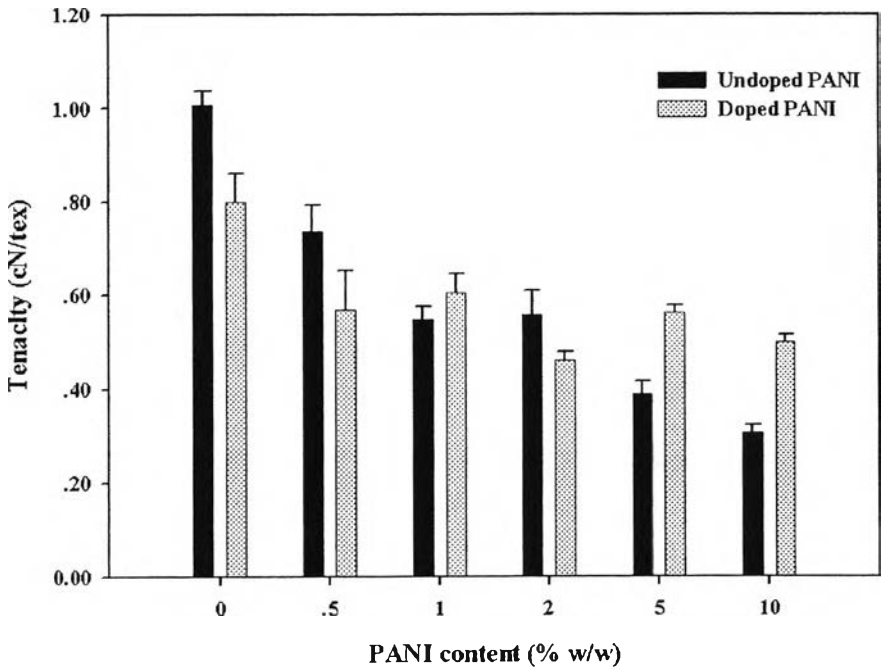

Figure 4.12 Tenacity of bundles of undoped and HCl-doped PANI/NR composite fibers with PANI contents of between 0 and 10 % w/w.

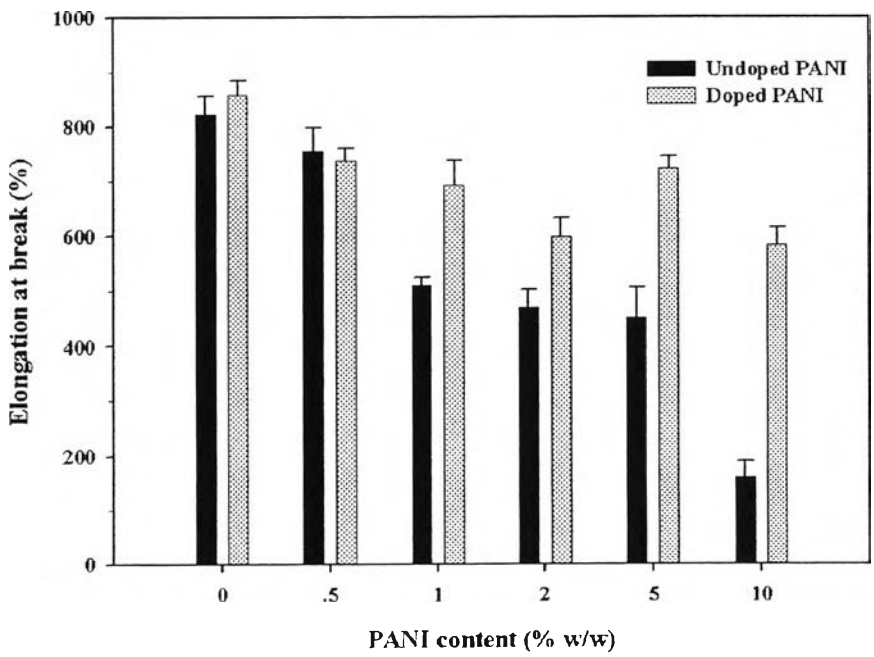

Figure 4.13 Elongation at break of bundles of undoped and HCl-doped PANI/NR composite fibers with PANI contents of between 0 and 10 % w/w.

4.2.6 Electrical Conductivity of Polyaniline/Natural Rubber Composite Fiber

4.2.6.1 Effect of Polyaniline Content and HCl-doping

The DC electrical conductivity of the PANI/NR composite fibers was studied as a function of PANI concentration and doping level using a conventional two-point probe arrangement. The results are plotted in Figure 4.14. In the case of the undoped composite fibers, the electrical conductivity increases gradually from 10^{-10} S/cm (neat NR fiber bundle with sodium alginate but no PANI) to 10^{-7} S/cm (10% w/w PANI) with increasing of PANI content. This finding os consistent with the finding by Camillo *et al.* (2005) who reported that NR latex itself was able partially to dope the PANI either by protonation from NR chains or by imparting conformational changes to the PANI chains. Upon doping with HCl, the electrical conductivity increases sharply for all PANI-containing fibers (but not the NR reference) and reaches a plateau of 1.02×10^{-3} S/cm at a PANI content of 5% w/w. Thus, the introduction of PANI promoted a conductivity increase of 7 orders without compromising the mechanical characteristics of the material in a major way. Further increase of the PANI concentration to 10% w/w increases the conductivity only marginally to 1.65×10^{-3} S/cm (Figure 4.14), suggesting that the percolation threshold is reached already at a PANI content of 5% w/w.

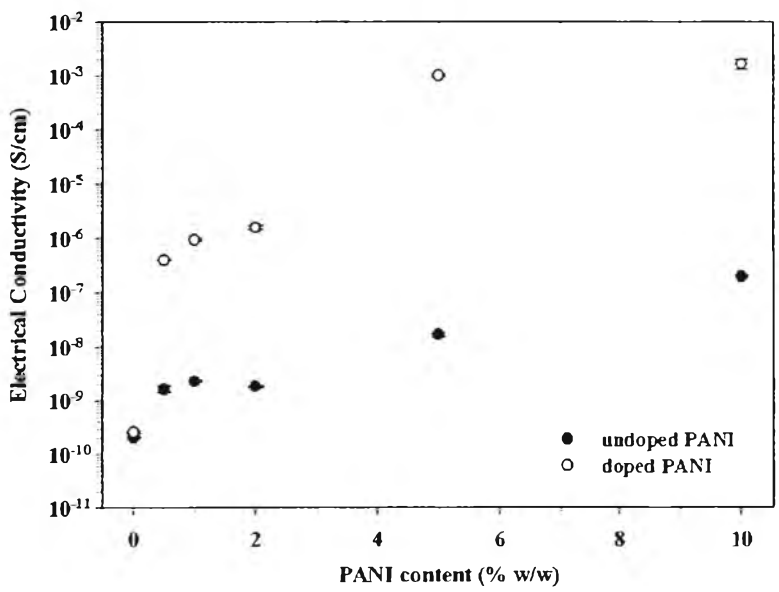

Figure 4.14 Electrical conductivity of undoped and HCl-doped PANI/NR composite fiber bundles as function of PANI content.

4.2.6.2 Effect of Strain Dependent Electrical Conductivity

Figure 4.15 shows the electrical conductivity of bundle of PANI/NR composite fibers containing 5% w/w HCl-doped PANI as a function of uniaxial strain $\varepsilon = L/L_o$-1. The initial conductivity slightly decreases under a low strain (<100%). This decrease may be due to the distance between the PANI particles or aggregates will be immediately increasing in response to the external force lead to disrupt the conducting pathways. Upon deformation of the strain of 100% up to 600%, the conductivity gradually increased until reaching a final value of 1.35×10^{-3} S/cm. This might imply that at high elongation, the PANI particles or aggregates were dispersed and distributed in a way of increased connection with each other resulting in an increase in electron tunnelling efficiency. In the light of classical percolation theory, these results provide further support for the conclusion that in the PANI/NR composite fibers studied here the PANI particles migrate to the fiber surfaces, where their higher-than-statistical density leads to percolation.

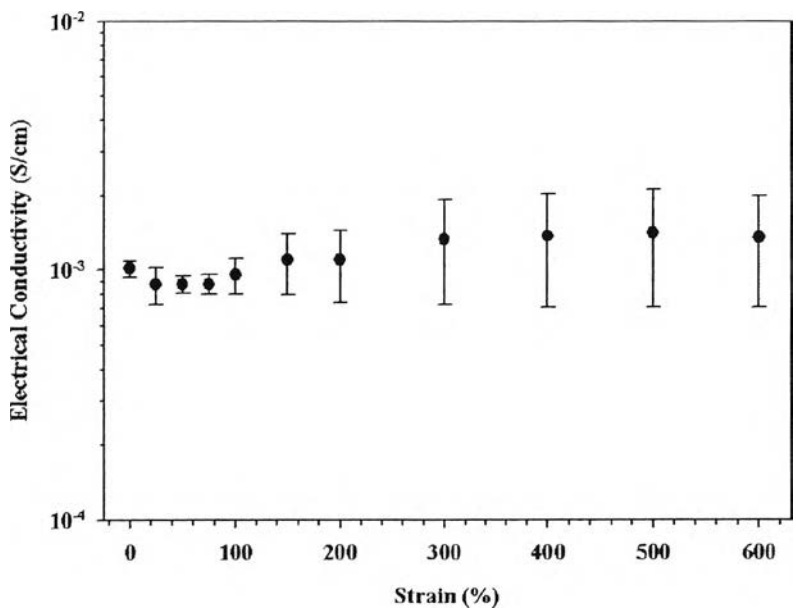

Figure 4.15 Electrical conductivity of HCl-doped PANI/NR composite fiber bundles comprising 5 % w/w PANI as a function of uniaxial strain.

4.2.7 Electromechanical Actuation of Polyaniline/Natural Rubber Composite Fiber

Finally, we explored the electromechanical actuation of PANI/NR composite fiber in terms of bending deformation under electric field. Figure 4.16 and Figure 4.17 show the bending of a neat NR fiber (without PANI) and HCl-doped PANI/NR composite with 5% w/w PANI content, respectively. In the both cases, the fibers significant bent toward the cathode under external electric field is applied. Since existing of the positive charges of calcium ions, as cross-linking agent of alginate network, in the matrix can be possible responded the bending direction to cathode side resulting from Coulomb interactions. We have measured the deflection, the distance between the free bottom end of the fiber with reference line, as a function of electric field intensity and time. These results analyzed from digital camera image are shown on Figure 4.18 and 4.19. In the case of neat NR fibers, they required electric field intensity up to 4.0 kV/cm in order to reach at a maximum deflection of 0.98 cm within response time of 81 S (Figure 4.18). Gratifyingly, in the case of 5% w/w HCl-doped PANI/NR composite, the electric field intensity only up to 1.4 kV/cm is required to reach a maximum deflection of 1.25 cm within response time of 48 S (Figure 4.19). It is obviously observed that incorporated PANI induced rapid bending deformation under lower electric field intensity than that of without PANI. We hypothesized that due to the PANI is in conducting state, posses the positive charge along the chain, so that it is possible to contribute in the bending to cathode. On the other hand, PANI particles are able to emit electrons as conductive polymer. As the electrons easily migrate to the anode, the fiber might be obtained a positive charge. Additionally, HCl-doped PANI, which has high dielectric constant, can be able to generate dipole-dipole interaction under electric field. The dipole-dipole interaction is possible to play a role in bending deformation. However, the detailed mechanism of the charge formation will be the subject of another study.

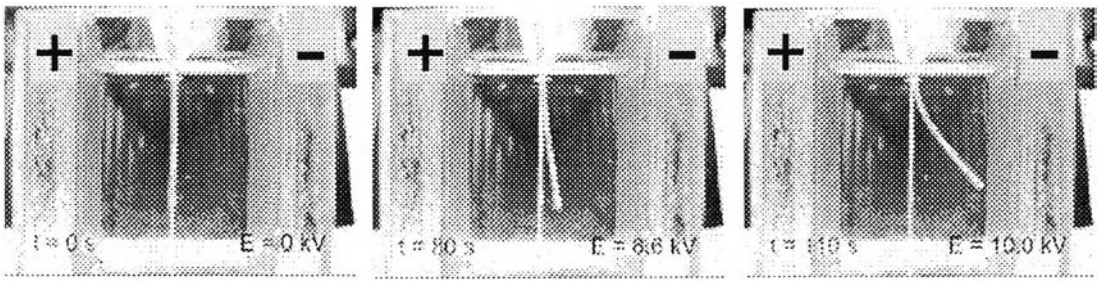

Figure 4.16 Captured digital camera images of bending of neat NR fiber bundle (without PANI but comprising sodium alginate).

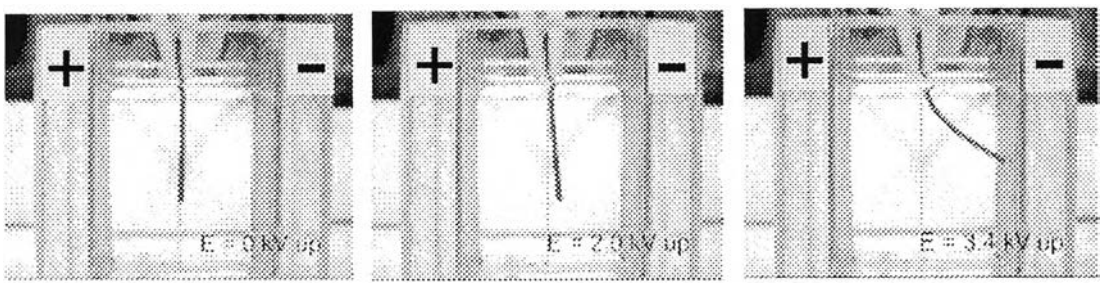

Figure 4.17 Captured digital camera images of bending of 5% w/w HCl-doped PANI/NR composite fiber bundle.

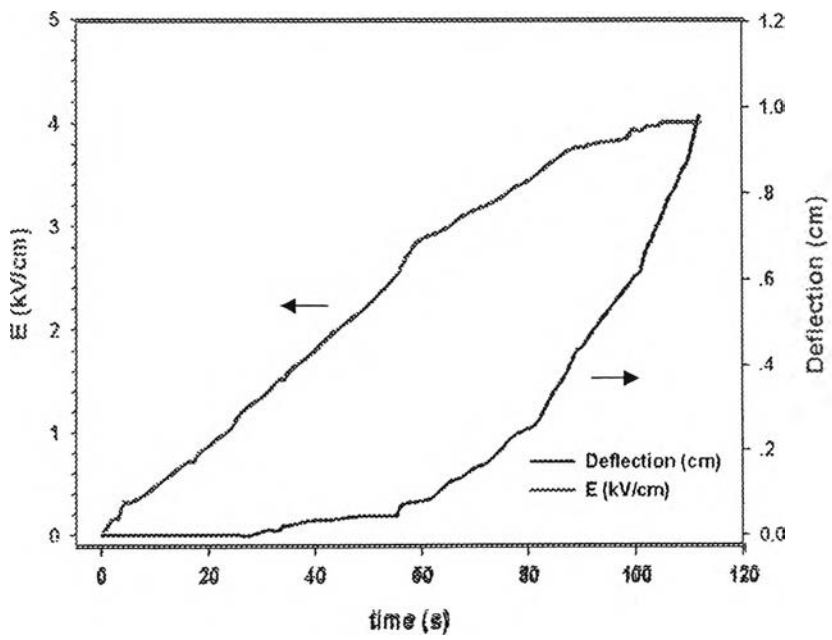

Figure 4.18 The deflection and required electrical field of neat NR fiber bundle.

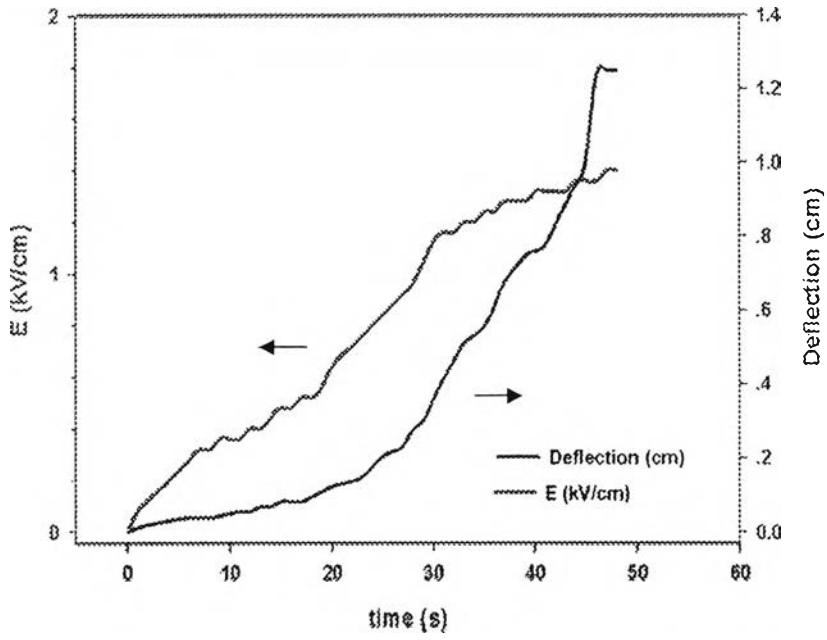

Figure 4.19 The deflection and required electric field of 5% w/w HCl-doped PANI/NR composite fiber bundle.